

Binding properties of apoferritin to nicotinamide and calcium

Fei Liu · Bingjian Du · Zhi Chai · Guanghua Zhao ·
Fazheng Ren · Xiaojing Leng

Received: 14 June 2012/Revised: 17 August 2012/Accepted: 28 August 2012
© Springer-Verlag 2012

Abstract The surface binding properties of apoferritin were investigated using two different substances, specifically, non-ionic nicotinamide and calcium. Nicotinamide could bind with apoferritin through hydrogen bonding. The binding location could be estimated by combining the Förster's non-radiation resonance energy transfer theory model and Molegro Virtual Docker docking software. The surface and internal cavities of apoferritin could be used to bind calcium through electrostatic attraction. Apoferritin monomers were stabilized only when the calcium concentration was lower than 20,000 μM , whereas a high calcium concentration could promote serious protein aggregation.

Keywords Apoferritin · Nicotinamide · Calcium · Load-carrying characteristics

Introduction

The development of nanovehicles as drug delivery systems has gained considerable interest in nutritional and pharmaceutical industries over the last several decades. Nanotoxicology research has indicated that the pharmacological properties, as well as biodegradability, biocompatibility,

and non-toxicity, of such new systems [1]. Therefore, synthetic nanovehicles, such as porous hollow silica nanoparticles [2], single-wall nanotubes [3], and C60 fullerenes [4] are often studied. Replacement of these synthetic materials with natural materials that are more acceptable to many people has become an attractive field of research.

Ferritin, a ubiquitous iron storage protein that plays a crucial role in intracellular iron homeostasis, has a 3-dimensional structure that is highly conserved among plants, animals, and bacteria. Ferritins have 24 similar or identical subunits arranged in a 4,3,2 symmetry, resulting in a hollow protein shell (outer diameter of 12–13 nm; inner diameter of 7–8 nm) where $\sim 4,500$ iron atoms can be stored as an inorganic complex. The iron cores in ferritin can be removed by dialysis against a solution containing a reducing agent. Ferritin without a ferrihydrite core is called apoferritin, the exterior and interior surfaces of which are amenable to both genetic and chemical modifications [5]. Aside from iron oxides, a variety of inorganic nanoparticles, such as $\text{Mn}(\text{O})\text{OH}$, $\text{Co}(\text{O})\text{OH}$, CdS , and ZnSe , have also been synthesized within the ferritin protein cage based on similar biomimetic strategies [6–9]. Works focusing on the interactions between apoferritin and small organic molecules have also been reported. Glucose, having a molecular cross-section of ~ 0.7 nm, can diffuse into the ferritin cavity over a period of several days [10]. The maximum size of molecules passing through the ferritin channels into the cavity is believed to be smaller than that of maltotriose (~ 2 nm) [11]. However, due to lack of extensive research, the discussion on the loading capacities of the apoferritin remains incomplete.

Nicotinamide (NA), which is part of the vitamin B group, is a precursor of nicotinamide adenine dinucleotide or its phosphate form, both of which are important

F. Liu · B. Du · Z. Chai · G. Zhao · F. Ren · X. Leng (✉)
CAU & ACC Joint-Laboratory of Space Food,
College of Food Science & Nutritional Engineering,
Key Laboratory of Functional Dairy Science of Beijing
and Ministry of Education, Beijing Higher Institution
Engineering Research Center of Animal Product,
The National Dairy Industry Technology System-Beijing
Innovation Team (NDITS-BIT), China Agricultural University,
No. 17 Qinghua East Road, Haidian 100083, Beijing, China
e-mail: xiaojing.leng@gmail.com

coenzymes in the redox reactions of living organisms. The pharmacological activities of NA, such as its anti-inflammatory properties and significant role during oxidative stress, DNA repair synthesis, and cerebral ischemia, among others, have been reported over the years [12–14]. Calcium, a mineral nutrient with many medical and healthcare uses, such as the treatment of bone loss [15], can fortify the nutritional values of food formulation [16]. In the present study, model samples of NA and calcium to represent non-ionic and ionic factors, respectively, were used to investigate the surface characteristics of apoferritin. The objective of this work is to determine the stability of apoferritin in the process of carrying drugs.

Materials and methods

Materials

Horse spleen ferritin (HoSF) and nicotinamide were purchased from Sigma-Aldrich (F4503, N0636). The 3-(N-morpholino) propanesulfonic acid (MOPS) was obtained from Amresco (USA). Ferrous sulfate, sodium dithionite, 2, 2'-bipyridyl were obtained from Sigma-Aldrich Co. (Beijing, PR China). All the reagents used were of analytical grade or purer (99.7 %).

Preparation of solutions

MOPS buffer solution (5 mM) was prepared by dissolving the powder in deionised water. The pH was adjusted to 7.0 with NaOH (1 M). ApoHoSF was prepared as described recently [17]. Protein solutions were obtained by dissolving an appropriate amount of each protein in the MOPS buffer solution (5 mM, pH 7.0). NA solutions (10 mM) were prepared with MOPS and stored at 4 °C. All protein concentrations were determined based on the Lowry method using BSA as a standard.

Fluorescence and UV-Vis spectrometry study

The fluorescence and UV-Vis intensities were recorded with a Varian Cary Eclipse fluorescence spectrophotometer and a Varian Cary 50 UV-Vis spectrophotometer (Varian Medical Systems, Inc., CA, USA), respectively. Fluorescence spectra were measured in the range of 290–400 nm at an excitation wavelength of 285 nm at 25 °C, using 5.0 nm excitation and 10.0 nm emission slit widths. Each spectrum was background corrected by subtracting the spectrum of the Milli-Q water and MOPS blank. The differential apoHoSF spectrum was obtained by subtracting the pure NA spectrum from the NA–apoHoSF mix spectrum.

Dynamic light scattering (DLS) measurements

DLS experiments were performed at 25 °C using a Viscotek model 802 dynamic light scattering instrument (Viscotek, Europe) as described previously [17]. The OmniSIZE 2.0 software was used to calculate the size/hydrodynamic radius (Rh) distribution of prepared proteins when protein samples were added certain amount of NA. All samples, unless stated otherwise the final concentration at 0.5 μM, were allowed to stand for 24 h prior to DLS measurement to ensure that the reactions were complete.

Scanning transmission electron microscopy (STEM)

Liquid samples were diluted with 5 mM Mops buffer (pH 7.0) prior to placing on carbon-coated copper grids and excess solution removed with filter paper; then, proteins were stained using 2 % uranyl acetate for 10 min. Transmission/Scanning electron micrographs (TEM/SEM) were imaged at 30 kV through a Hitachi S-5500 scanning electron microscope.

3D molecular models and molecular docking

ChemBioOffice ultra 2008 (v.11.0) (<http://www.cambridgesoft.com/software/ChemBioOffice>), Pymol (<http://www.pymol.org>) and MVD (Molegro Virtual Docker, 8.0 <http://www.molegro.com>) were used here for molecular structure construction and molecular docking. The MVD is based on a new heuristic search algorithm that combines differential evolution with a cavity prediction algorithm. During the search process, fast and accurate identification of the potential binding modes is achieved through the use of predicted cavities.

The 3-dimensional structure of the NA was initially optimized by ChemBioOffice with MM2 method combined in with default set, then displayed by pymol. The 3-dimensional structures of apoHoSF (1IER) were loaded from their worldwide protein data bank (PDB) (<http://www.rcsb.org/pdb/home/home.do>) elucidated structures. The docking of peptides to NA was performed according to the guidance of MVD.

For the complex, the atom types and the bond orders were corrected to both ligand and protein structures using the MVD automatic preparation function, and the MVD default charges were assigned. Potential binding sites (cavities) were detected using the grid-based cavity prediction algorithm. The population size, maximum interactions, scaling factor, and crossover rate were set to 150, 2000, 0.50, and 0.90, respectively. For each complex, we performed 100 independent runs with the MolDock optimizer algorithm, with each run returning one solution (pose).

Statistical analysis

Statistical data were analyzed using origin 8.0. Statistics on a completely randomized design were performed using the general linear models procedure with the One-way analyses of variance (ANOVA), Duncan's multiple range test ($P < 0.05$) was used to detect differences among mean values.

Results and discussion

UV-visible and fluorescence spectroscopy

UV-visible and fluorescence techniques were used to analyze the properties of the chromophoric and fluorophoric groups, which are often involved in various intermolecular reactions. Fluorescence quenching processes usually refer to two modes, namely, dynamic and static. Dynamic quenching occurs when the excited fluorophore collides with an atom or molecule that can facilitate non-radiative transitions to the ground state. Static quenching implies either the existence of a spherical region of effective quenching or the formation of a non-fluorescent complex. Empirically, a linear expression (Eq. 1) can be used to describe the variation of the fluorescence versus the concentration of the quencher [18]:

$$F_0/F = 1 + K[Q] \quad (1)$$

where F_0 and F represent the fluorescence intensity without and with the quencher, respectively. K is the quenching constant, which is equivalent to the reaction constant, and $[Q]$ is the quencher concentration. Combination of the fluorescence and absorption spectra could provide information with which to analyze the characteristics of the dynamic and static mode quenching [19].

At an excitation wavelength of 285 nm, apoHoSF showed maximum intrinsic fluorescence around 320 nm caused by Trp residues [19]. The fluorescence of Tyr residues (304 nm) at this excitation wavelength was very weak and thus neglected. Figure 1 exhibits variations in the apoHoSF fluorescence spectrum versus the NA concentration, where the intensity of the apoHoSF fluorescence decreases with increasing NA concentration. Figure 2 compares the UV-visible spectra of the pure NA, apoHoSF, and NA-apoHoSF. The NA-apoHoSF spectrum does not overlap with superposition of apoHoSF and NA separately, indicating the formation of a NA-apoHoSF complex. In addition, the UV absorption values for NA at the excitation and emission wavelength of apoferritin were minor, thus the inner-filter effect was assumed to be limited. The decrease in fluorescence is mainly attributed to quenching by NA [20]. Figure 3 shows a linear Stern-Volmer relationship obtained by fitting

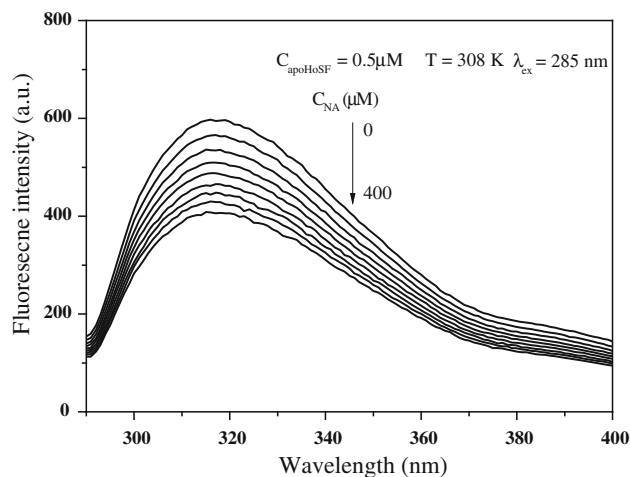


Fig. 1 Fluorescence spectra of apoHoSF and NA-apoHoSF systems (pH 7.0). The concentration of apoHoSF was 0.5 μM . $\lambda_{\text{ex}} = 285 \text{ nm}$

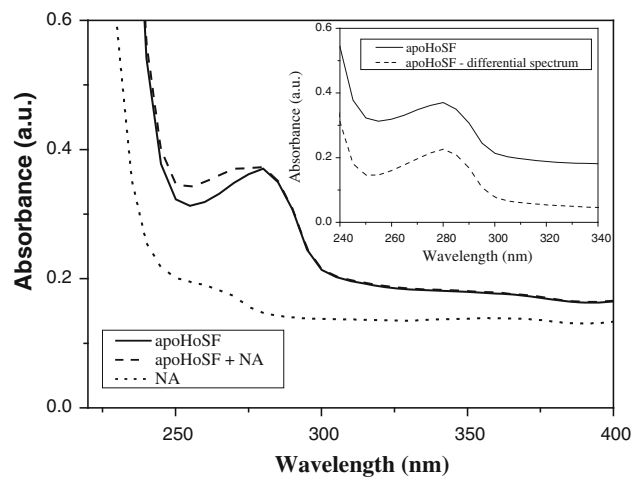


Fig. 2 Absorption spectra of NA, apoHoSF and NA-apoHoSF (pH 7.0). The concentrations of apoHoSF and NA were 0.5 and 200 μM , respectively. The insert was the comparison of the differential apoHoSF spectrum and the pure apoHoSF spectrum

Eq. 1 to the experimental data. Taking into account the collision quenching constant, which is normally lower than $2 \times 10^2 \text{ l mol}^{-1}$ [21], the NA-apoHoSF mode likely became more static.

The thermodynamic parameters of enthalpy (ΔH) and entropy (ΔS) of NA-apoHoSF interactions are important in confirming the binding mode of the reaction. The variation in binding enthalpy ΔH , which is assumed not to change with temperature, was calculated using the classical Van't Hoff equation (Eq. 2) [22, 23]:

$$\ln\left(\frac{K_2}{K_1}\right) = -\frac{\Delta H}{R} \left(\frac{1}{T_2} - \frac{1}{T_1}\right) \quad (2)$$

where T is the temperature and R is the ideal gas constant. The binding free energy ΔG was calculated using:

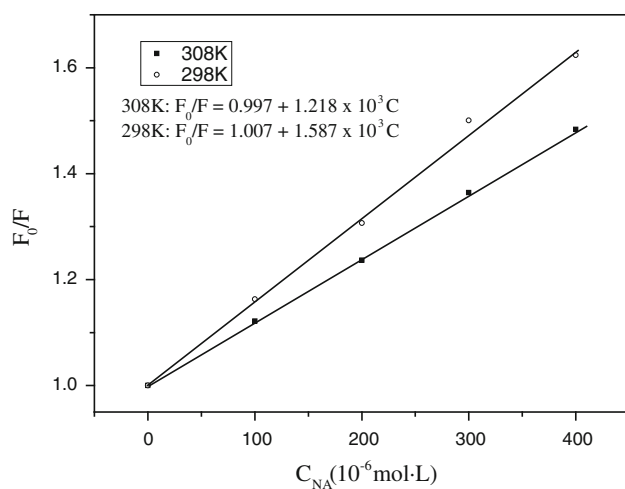


Fig. 3 Stern–Volmer curves of apoHoSF with certain amount of NA

Table 1 Thermodynamic binding parameters of NA–apoHoSF system

T/K	$K(\text{L mol}^{-1})$	$\Delta H/\text{kJ mol}^{-1}$	$\Delta S/\text{J mol}^{-1} \text{K}^{-1}$	$\Delta G/\text{kJ mol}^{-1}$
298	1.59×10^3	-20.21	-6.54	-18.26
308	1.22×10^3			-18.19

$$\Delta G = -RT \ln K \quad (3)$$

The variation in binding entropy ΔS was calculated with $\Delta G = \Delta H - T\Delta S$, and the results were summarized in Table 1.

The negative ΔG indicates that the binding of NA and apoHoSF is energetically favorable, while the negative ΔS and ΔH indicate that the binding behaviors decrease the entropy of the molecular environment of Trp and that the reaction is exothermic. This reaction is seen as a result of hydrogen bonding and van der Waals power [24].

According to Förster's non-radiation resonance energy transfer theory (FRET), the energy transfer occurs only when the fluorescence emission spectra of the donor and the absorption spectra of the acceptor have overlap and the distance between donor and acceptor is not longer than 7 nm. The following equations could be used to estimate the distance between the acceptor and donor [25]:

$$E = \frac{R_0^6}{R_0^6 + r^6} = 1 - \frac{F}{F_0} \quad (4)$$

$$R_0^6 = 8.8 \times 10^{-25} (K^2 \varphi N^{-4} J) \quad (5)$$

$$J = \frac{\int_0^\infty F_D(\lambda) \varepsilon_A(\lambda) \lambda^4 d\lambda}{\int_0^\infty F_D(\lambda) d\lambda} \quad (6)$$

In these equations, E is the efficiency of transfer between the donor and the acceptor, R_0 is the critical distance when the efficiency of transfer reaches 50 %, r is the distance between the acceptor and the donor, K^2 is the space factor of

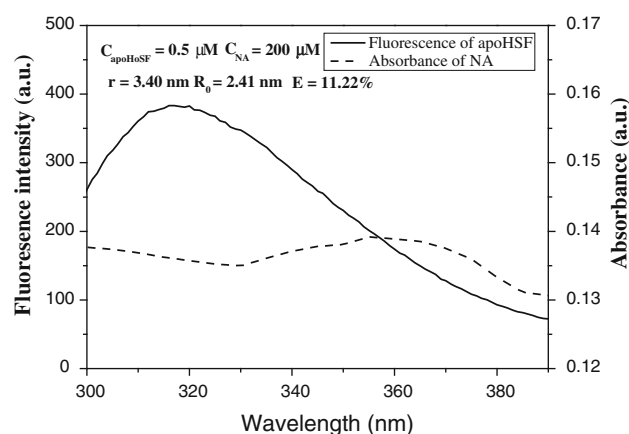


Fig. 4 Absorption spectrum of NA and fluorescence emission spectrum of apoHoSF

orientation, N is the refracted index of medium, φ is the fluorescence quantum yield of the donor, J is the effect of the spectral overlap between the emission spectrum of the donor and the absorption spectrum of the acceptor, $F_D(\lambda)$ is the corrected fluorescence intensity of the donor in the wavelength range λ_0 to λ , and $\varepsilon_A(\lambda_0)$ is the extinction coefficient of the acceptor at λ_0 . The overlap integral J can be evaluated by integrating the spectra in Fig. 4 according to Eq. 6. Under the present experimental conditions, using $K^2 = 2/3$, $N = 1.336$, and $\varphi = 0.118$ [26], the obtained distance between NA and Trp in apoHoSF was about 3.40 nm.

Molecular docking of NA to apoHoSF

The space volume of NA was defined as 38 according to the lengths of the molecular bonds. Using MVD docking software, apoHoSF was identified to have about 100 cavities as binding sites, which could be divided into 4 main classes: (1) 8 threefold channels with space volumes varying between 151 and 215, (2) 24 intersubunit gaps with a volume of 71, (3) 24 cavities on the surface of subunits with volumes varying between 49 and 57, and (4) 6 fourfold channels with a volume of 23. The rest of the cavities had volumes less than 23. By comparing space volumes, the large threefold channels may allow NA molecules to enter apoHoSF. The cavities on the surface of the subunit and intersubunit gap are able to bind with NA but such an occurrence could be reduced by steric hindrance. Sites with volumes less than 23 were very small so they were neglected. Analysis of fluorescence and adsorption indicates that the NA binding sites were in the vicinity of the Trp residues. Thus, the most likely binding sites of NA on apoHoSF are proposed in Fig. 5. The cavity of the binding site was formed by Arg(75), Phe(35), Ser(32), Arg(39), Asp(87), and Ala(76). Hydrogen bonds were formed between the amino hydrogen of Ala(76) and the pyridine

Fig. 5 Illustration of the structural formulae of NA (a), the diagram of binding site of NA (yellow) on apoHoSF (b) and 3-dimensional structure of apoHoSF banded by NA (c). Red-fluorescence group (Trp), green-NA

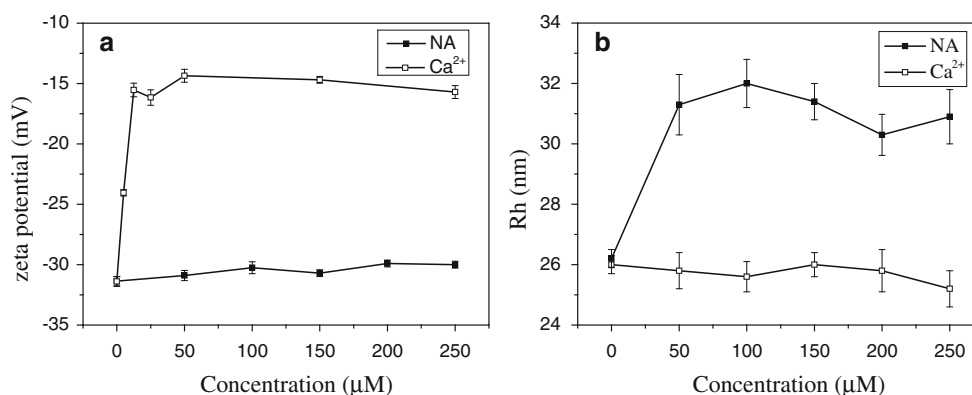
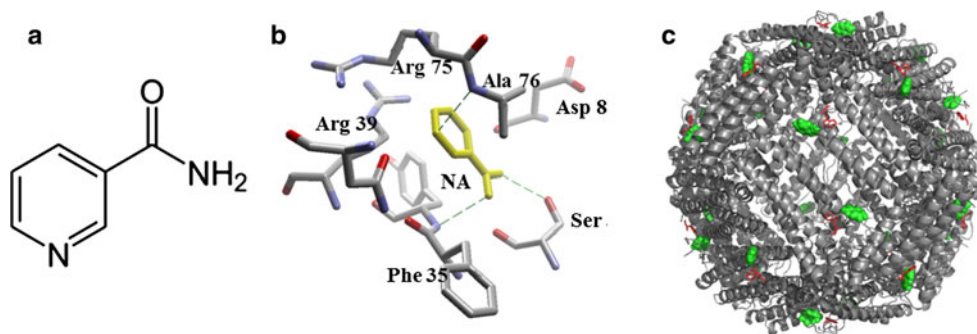


Fig. 6 Zeta and size variation of the NA–apoHoSF and Ca²⁺–apoHoSF system (pH 7.0). **a** Zeta potential; **b** size measurement. The concentration of apoHoSF was 0.5 μM

nitrogen of NA, the –NH of Phe(35) and the carbonyl oxygen of NA, and the carbonyl oxygen of Ser(32), and the amino nitrogen of NA. Water molecules could also serve as a bridge to produce other hydrogen bonds. Some basic residues, such as Arg(75), Arg(39), and Ala(76), were in very close proximity to NA, which suggests that a strong hydrophobic interaction also exists in the binding process.

Zeta size and potential measurements

The most significant difference between the NA–apoHoSF and Ca²⁺–apoHoSF systems involves the variation in their protein charge states. Figure 6 compares the variations of the size and zeta potential, ζ , of apoHoSF and the concentrations of calcium and NA at pH 7. The ζ of pure apoHoSF was approximately –33 mV. The negative charges were mainly from the amino acid residues Glu and Asp. The ζ of the apoHoSF system was independent of the NA concentration (Fig. 6a). The stable ζ value of NA–apoHoSF system is due to the non-ionic NA (pK = 3.6) [27]. Hydrogen bonding was the main binding forces between the non-ionic NA and apoHoSF. In contrast, addition of 50 μM calcium could reduce the ζ of apoHoSF to –15 mV through electrostatic neutralization. This ζ was maintained until the

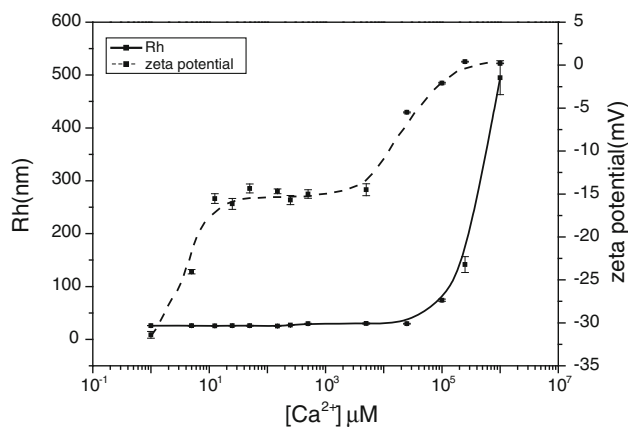


Fig. 7 Zeta and size variation of the Ca²⁺–apoHoSF system (pH 7.0). The concentration of apoHoSF was 0.5 μM

calcium concentration was over 5,000 μM (Fig. 7). When the calcium concentration reached 300,000 μM, apoHoSF was completely neutralized.

The hydrodynamic size (R_h) of apoHoSF was measured using dynamic light scattering spectroscopy. The size of apoHoSF was slightly increased with the presence of NA (Fig. 6b). When the calcium concentration was less than

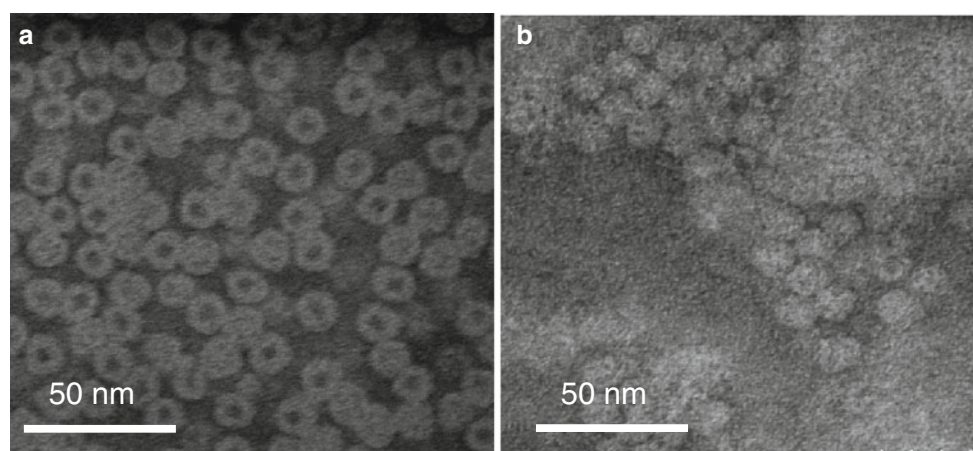


Fig. 8 STEM images of the NA-apoHoSF (a) and Ca^{2+} -apoHoSF (b) system. The concentration of apoHoSF was 0.5 μM

20,000 μM , the size of apoHoSF was maintained at 26 nm. Rapid aggregation of proteins could be induced when the total charges are neutralized by calcium (Fig. 7). Figure 8 exhibits STEM photographs of the (a) NA-apoHoSF and (b) Ca^{2+} -apoHoSF systems. The dark center of the NA-apoHoSF monomer is caused by uranium dye. In the Ca^{2+} -apoHoSF system, the internal negatively charged cavity of the protein is filled with Ca^{2+} , which could hamper the entry of uranium [28]. Similar observations have also been reported in CCMV (Cowpea chlorotic mottle virus) [29].

Conclusions

The present results indicate that apoferritin could be used to load a variety of functional factors. Non-ionic molecules, such as nicotinamide, could bind with apoferritin through hydrogen bonding. The binding location could be estimated by combining the FRET model and MVD docking software. The surface and internal cavities of apoferritin could be used to bind calcium through electrostatic attraction. Apoferritin monomers were stabilized only when the calcium concentration was lower than 20,000 μM , whereas a high calcium concentration could promote serious protein aggregation.

Acknowledgments This research was supported by National Natural Science Foundation of China (NSFC) (No. 31171771) and National Science and Technology Support Program (2011BAD23B04). The authors acknowledge Prof. Yunjie Yan (Beijing National Center for Microscopy, Tsinghua University, Beijing, China) for his technical advice.

References

1. Shevchenko EV, Talapin DV, Kotov NA, O'Brien S, Murray CB (2006) Structural diversity in binary nanoparticle superlattices. *Nature* 439(7072):55–59
2. Chen JF, Ding HM, Wang JX, Shao L (2004) Preparation and characterization of porous hollow silica nanoparticles for drug delivery application. *Biomaterials* 25(4):723–727
3. Mamalis A, Vogtländer L, Markopoulos A (2004) Nanotechnology and nanostructured materials: trends in carbon nanotubes. *Precision Engineering* 28(1):16–30
4. Becker L, Poreda RJ, Bunch TE (2000) Fullerenes: an extraterrestrial carbon carrier phase for noble gases. *Proc Natl Acad Sci* 97(7):2979
5. Tsapikouni TS, Missirlis YF (2008) Protein–material interactions: from micro-to-nano scale. *Mater Sci Eng, B* 152(1):2–7
6. Uchida M, Klem MT, Allen M, Suci P, Flenniken M, Gillitzer E, Varpness Z, Liepold LO, Young M, Douglas T (2007) Biological containers: protein cages as multifunctional nanoplatfoms. *Adv Mater* 19(8):1025–1042
7. Douglas T, Stark VT (2000) Nanophase cobalt oxyhydroxide mineral synthesized within the protein cage of ferritin. *Inorg Chem* 39(8):1828–1830
8. Okuda M, Kobayashi Y, Suzuki K, Sonoda K, Kondoh T, Wagawa A, Kondo A, Yoshimura H (2005) Self-organized inorganic nanoparticle arrays on protein lattices. *Nano Lett* 5(5):991–993
9. Iwahori K, Yoshizawa K, Muraoka M, Yamashita I (2005) Fabrication of ZnSe nanoparticles in the apoferritin cavity by designing a slow chemical reaction system. *Inorg Chem* 44(18):6393–6400
10. May M, Fish W, Brown E, Aisen P, Fielding J (1977) The restrictive nature of apoferritin channels as measured by passive diffusion. *Proteins Iron Metab* 31–38
11. Yang D, Nagayama K (1995) Permeation of small molecules into the cavity of ferritin as revealed by proton nuclear magnetic resonance relaxation. *Biochemical Journal* 307:253–256
12. Chaidemenos GC (2001) Tetracycline and niacinamide in the treatment of blistering skin diseases. *Clin Dermatol* 19(6):781–785
13. Chong ZZ, Lin SH, Maiese K (2002) Nicotinamide modulates mitochondrial membrane potential and cysteine protease activity during cerebral vascular endothelial cell injury. *J Vasc Res* 39(2):131–147
14. Klaidman L, Morales M, Kem S, Yang J, Chang ML, Adams JD Jr (2003) Nicotinamide Offers Multiple Protective Mechanisms in Stroke as a Precursor for NAD^+ , as a PARP Inhibitor and by Partial Restoration of Mitochondrial Function. *Pharmacology* 69(3):150–157
15. Pak CYC, Avioli LV (1988) Factors affecting absorbability of calcium from calcium salts and food. *Calcif Tissue Int* 43(2):55–60

16. Fang Y, Tung M, Britt I, Yada S, Dalgleish D (2002) Tensile and barrier properties of edible films made from whey proteins. *J Food Sci* 67(1):188–193
17. Li C, Fu X, Qi X, Hu X, Chasteen ND, Zhao G (2009) Protein Association and Dissociation Regulated by Ferric Ion. *J Biol Chem* 284(25):16743
18. Fang R, Jing H, Chai Z, Zhao GH, Ren FZ, Liu F, Leng XJ Design and characterization of protein-quercetin bioactive nanoparticles. *J Nanobiotechnol* 9(19)
19. Lakowicz JR (2006). In: BR M (ed) Principles of fluorescence spectroscopy. Springer, New York
20. Van De Weert M (2010) Fluorescence quenching to study protein-ligand binding: common errors. *Journal of fluorescence* 20(2):625–629
21. Michon J, Frelon S, Garnier C, Coppin F (2010) Determinations of uranium (VI) binding properties with some metalloproteins (transferrin, albumin, metallothionein and ferritin) by fluorescence quenching. *Journal of fluorescence* 20(2):581–590
22. Bai Z, Lodge TP (2009) Thermodynamics and Mechanism of the Block Copolymer Micelle Shuttle between Water and an Ionic Liquid. *J Phys Chem B* 113(43):14151–14157
23. Subbaiah MV, Vijaya Y, Kumar NS, Reddy AS, Krishnaiah A (2009) Biosorption of nickel from aqueous solutions by *Acacia leucocephala* bark: kinetics and equilibrium studies. *Colloids Surf, B* 74(1):260–265
24. Ross PD, Subramanian S (1981) Thermodynamics of protein association reactions: forces contributing to stability. *Biochemistry* 20(11):3096–3102
25. Förster T (1948) Intermolecular energy transference and fluorescence. *Ann Physik* 2:55–75
26. Ghosh SK, Hossain SU, Bhattacharya S, Bhattacharya SC (2005) 2-(2-Selenocyanic acid ethyl ester)-1 H-benz [de] isoquinoline-1, 3-(2H)-dione, synthesis photophysics and interaction with bovine serum albumin: a spectroscopic approach. *J Photochem Photobiol, B* 81(2):121–128
27. Korchagin V, Tomashchik A, Vasil'ev V (1971) Differential titration of the monosodium salt of novobiocin and nicotinamide in a medium of nonaqueous solvents. *Pharm Chem J* 5(8):501–504
28. Masuda T, Goto F, Yoshihara T, Mikami B (2010) Crystal structure of plant ferritin reveals a novel metal binding site that functions as a transit site for metal transfer in ferritin. *J Biol Chem* 285(6):4049
29. Douglas T, Young M (1998) Host–guest encapsulation of materials by assembled virus protein cages. *Nature* 393(6681): 152–155